Overview of JT-60U Results toward High Integrated Performance in Reactor-Relevant Regime

T. Fujita, JT-60Team

Japan Atomic Energy Research Institute, Naka Fusion Research Establishment
Naka-machi, Naka-gun, Ibaraki-ken, Japan.

e-mail contact of main author: fujitat@fusion.naka.jaeri.go.jp

Abstract. Recent JT-60U results toward high integrated performance are reported with emphasis on the projection to the reactor-relevant regime. N-NB and EC power increased up to 6.2 MW and 3 MW, respectively. A high β_p H-mode plasma with full non-inductive current drive has been obtained at 1.8 MA and the fusion triple product reached 3.1×10^{20} m^{-3}keVs. High beta with β_N =2.7 was maintained for 7.4 s. NTM suppression with EC was accomplished using a real-time feedback control system and improvement in β_N was obtained. A stable existence of current hole was observed. High DT-equivalent fusion gain of 0.8 was maintained for 0.55 s in a plasma with a current hole. The current profile control in high bootstrap current reversed shear plasmas was demonstrated using N-NB and LH. A new operation scenario has been established in which a plasma with high bootstrap current fraction and ITBs is produced without the use of OH coil. ECCD study was undertaken in a reactor-relevant high T_e regime. A new type of AE mode has been proposed and found to explain the observed frequency chirp quite well. High confinement reversed shear plasmas with $T_e > T_i$ were obtained. Ar exhaust with EC heating was obtained in a high β_p mode plasma. Impurity accumulation related to strong ITBs in a reversed shear plasma and degradation of ITB by ECH in a weak positive shear plasma have been found. Dedicated measurement of ELM dynamics and SOL plasma flow advanced the physics understanding. N-NB heating in an Ar-seed plasma extended the density region to 95% of Greenwald density with HH_{y2}=0.9. The enhancement of pedestal pressure was obtained with an increase of β_p in a high triangularity configuration.

1. Introduction

The main purpose of JT-60U project is to establish scientific basis for ITER and demo tokamak reactor. Our ultimate goal is to achieve and sustain high integrated performance, namely high beta, high confinement, high bootstrap current fraction, full non-inductive current drive and heat/particle control, in a reactor-relevant regime. We have developed weak magnetic shear ("high β_p mode") [1,2] and reversed magnetic shear [3] plasmas toward this goal [4]. In both regimes, the internal transport barrier (ITB) [5,6] and the edge pedestal are obtained simultaneously. As a large-sized tokamak equipped with a variety of devices for heating, current drive and profile control, JT-60U has high ability to approach the conditions required in reactors (ITER or demo): low values of normalized Larmor radius and collisionality, high toroidal field, high temperature with $T_e > \sim T_i$, small central fueling, small ELM activities, etc. This paper reports recent JT-60U results, after the last IAEA conference [7], with emphasis on the projection to the reactor-relevant regime.

2. Improved Machine Status

The JT-60U tokamak has a large variety of heating and current drive systems, which consist of the conventional positive-ion-based neutral beams (P-NBs, co- and counter-tangential and perpendicular injection), high-energy tangential negative-ion-based neutral beams (N-NBs), LHRF, ICRF and ECRF systems. The N-NB provides, in addition to the current drive, the electron heating through high-energy ions with small particle fueling, and can simulate the plasma heating and/or excitation of Alfvén instability by α particles in reactors. The ECRF system enables us to vary the ratio of T_e/T_i in a wide region including the reactor-relevant regime ($T_e > \sim T_i$) by efficient on-axis electron heating.

In the N-NB system, the beam deflection and uniformity of the source plasma have been improved. The increased acceleration current resulted in the injection power of 6.2 MW with
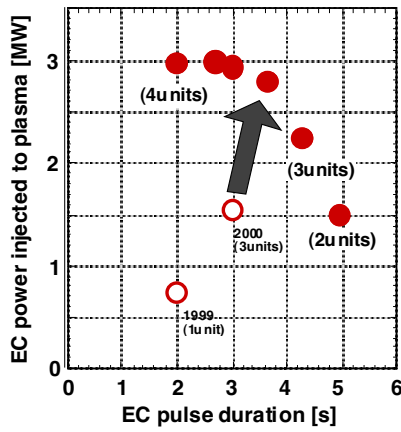
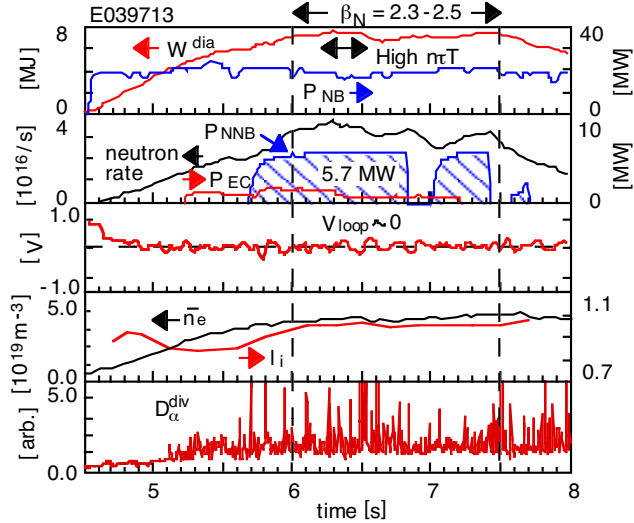FIG. 1. Progress in EC power injected into the plasma and in its pulse width.

FIG. 2. Waveforms of the high β_p H-mode discharge E39713.

the injection energy of 381 keV and the pulse length of 1.7 s. The improved beam divergence extended the pulse length and the long pulse injection for 10 seconds has been achieved at 355 keV and 2.6 MW with one ion source [8]. In the 110 GHz ECRF system, a new unit has been installed in addition to previous three units in 2001. The antenna for this unit is independent from the antenna for previous three units and the injection angle can be scanned toroidally as well as poloidally. Each unit has one gyrotron whose output power is ~ 1 MW. The torus-injected EC power is plotted as a function of pulse length in Fig.
1. The injected power reached 3 MW, twice as large as before 2000, for 2.7 s and the injected energy reached 10 MJ (2.8 MW for 3.6 s) .

The core fueling with pellets and the plasma shape control are also important for improving the plasma performance. In the multiple pellet injector system [9,10], injection from a high-field-side equatorial plane has been made possible, in addition to a high-field-side top injection, in which efficient fueling is expected in terms of the effect of ExB drift. The capacity of poloidal coils for control of plasma triangularity δ has been expanded by raising their maximum current from 40 kA to 48 kA and the pulse length from ~5 s to ~10 s for 40 kA.

These improvements have enhanced our capability of current drive, profile control and shape control.

3. Improved Performance in High β_p H-mode and Sustainment of High β_N

In the high β_p H-mode, the full non-inductive current drive with ~50% of bootstrap current fraction at the plasma current of 1.5 MA was realized in 2000 with N-NB injection [7]. The current drive efficiency of N-NB reached 1.55×10^{19} $Am^{-2}W^{-1}$ with increased $T_e(0)$ of 13 keV by the EC heating. High beta ($\beta_N = 2.5$) and high confinement ($HH_{y2} = 1.4$) were also obtained.

In 2001, extension to higher current regime of full non-inductive current drive was pursed by utilizing the increased N-NB power and increased current in poloidal coils for higher triangularity. As a result, the full non-inductive current drive has been achieved in a 1.8 MA high β_p H-mode plasma shown in Fig. 2 [11]. In this discharge, N-NB with 5.7 MW and 402 keV was injected and high beta ($\beta_N = 2.4$) and high confinement ($HH_{y2} = 1.2$) were maintained. At t = 6.5 s, the bootstrap current fraction (f_{BS}) was 50% and the NBCD+ECCD fraction was 50%. The fusion triple product and DT-equivalent fusion gain reached 3.1×10^{20} $m^{-3}keVs$ ($n_D(0) = 4.2 \times 10^{19}$ m^{-3}, $T_i(0) = 21.5$ keV, $\tau_E = 0.344$ s) and 0.185, respectively. Other parameters are listed in Table I. The value of fusion triple product renewed remarkably

the previous record under the full non-inductive current drive, 2×10^{20} m^{-3}keVs. The toroidal field and the normalized Larmor radius also approached the reactor-relevant regime.

The sustainable beta in high β_p H-mode plasmas is limited by neoclassical tearing modes (NTMs) with m/n = 3/2 and/or 2/1. In the discharge shown in Fig. 2, NTM was suppressed by tailoring the pressure and current profiles so that the steep gradient is not located at the mode rational surface, namely q = 1.5 and 2. Long sustainment of high β_N approaching the current diffusion time scale was undertaken in a lower current regime, where higher triangularity can be maintained for longer time. The improvement of

FIG. 3. Progress in sustained β_N.

capacity of poloidal field coils enables us to maintain $\delta\sim0.4$ for 10 s at the plasma current of 1 MA. In a shot E39511, $\beta_N\sim2.7$ was maintained for 6.5 s or $45\tau_E$ without appearance of NTM. To avoid the large heat load to the first wall due to the shine-through power of perpendicular NBs, the plasma density was kept relatively high, namely 67% of the Greenwald density, by injecting pellets continuously. The high density may result in the moderate confinement, HH$_{y2}\sim0.9$. Figure 3 indicates sustained β_N as a function of its duration. The duration of β_N =2.7, which is required for the steady-state operation scenario in ITER [12], was extended remarkably. In another shot E39706, longer sustainment (7.4 s or $60\tau_E$) of β_N = 2.7 was also achieved, though the confinement was lower due to the continuous m/n=3/2 NTM. The cause of appearance of NTM in this discharge is attributed to slightly higher $\beta_N\sim3$ in the initial phase of heating. In these long-pulse discharges, the density was kept constant and no accumulation of impurities was observed. In shorter pulse length, we can obtain higher current for δ control coil and hence higher δ. The quasi-steady beta values (maintained for longer than $5\tau_E$) has been raised to β_N = 3.05 by the increase of δ to 0.6.

To sustain high β_N in a low collisionality (ν_e^*) regime, suppression of NTM is required. A system for real-time NTM detection and EC wave injection has been developed and
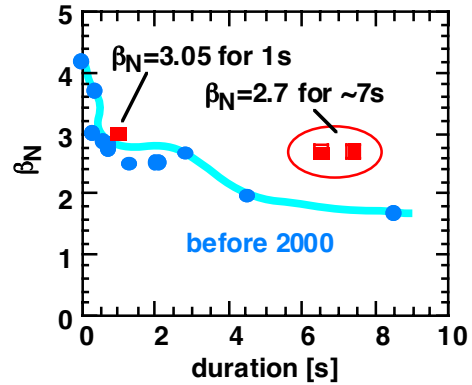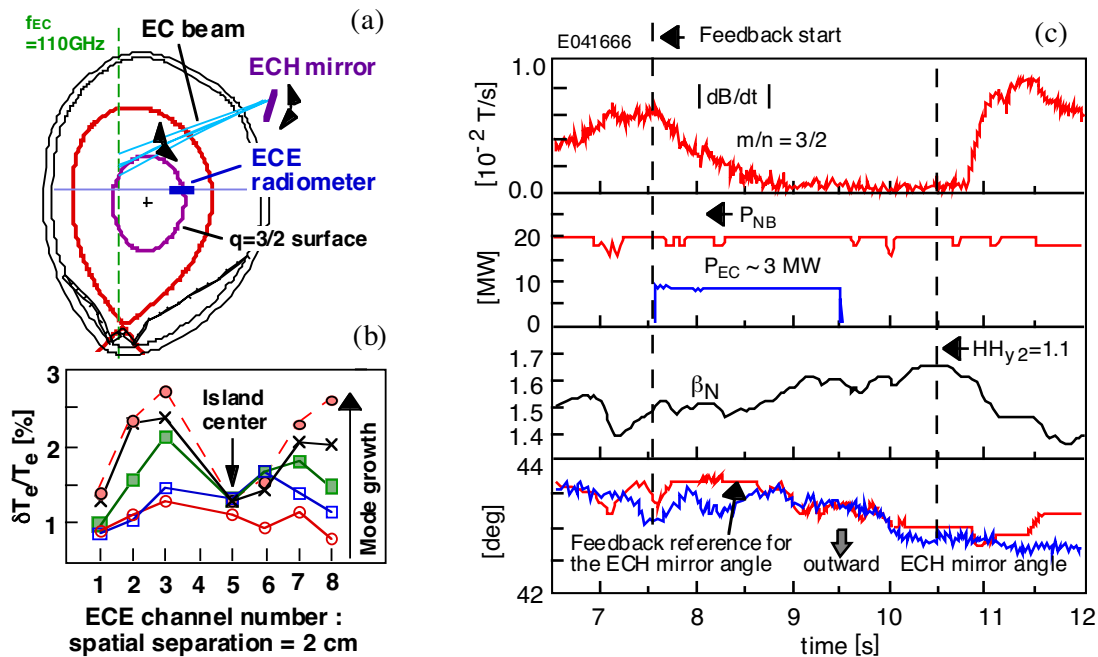

FIG. 4. NTM suppression experiment. (a) Schematic view of the system. (b) Profile of electron temperature perturbation. (c) Waveforms of a typical discharge.
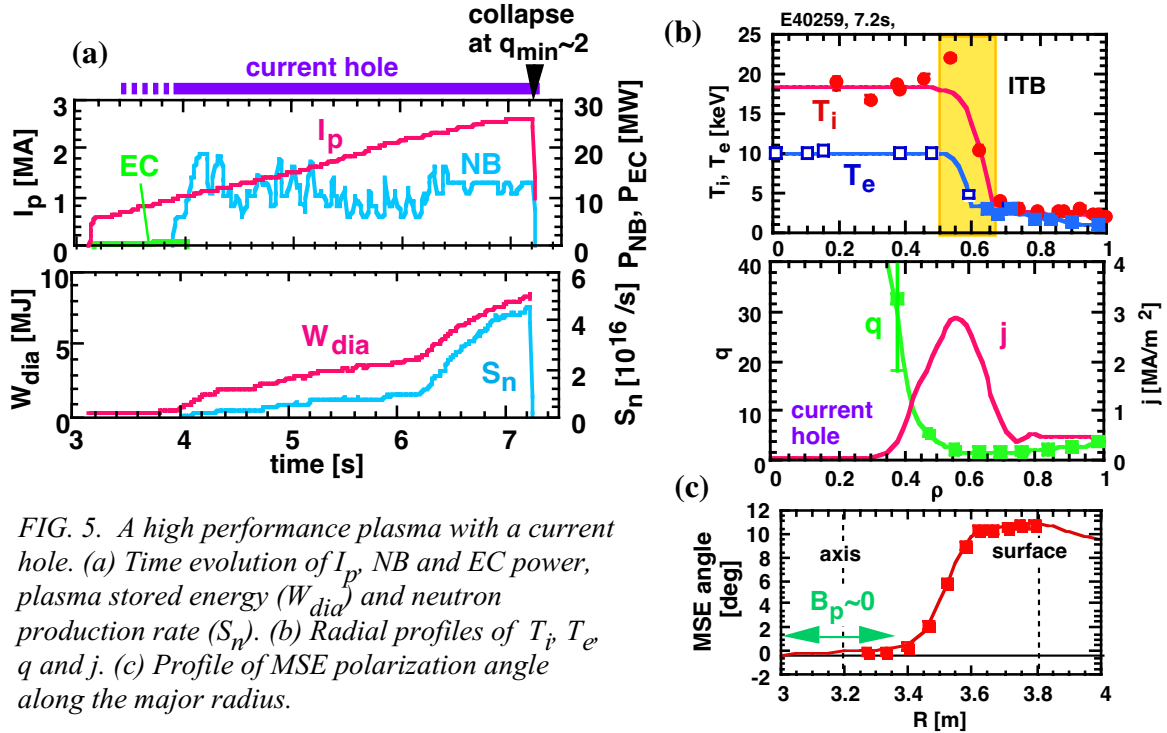
FIG. 5. *A high performance plasma with a current hole. (a) Time evolution of I_p, NB and EC power, plasma stored energy (W_{dia}) and neutron production rate (S_n). (b) Radial profiles of T_i, T_e, q and j. (c) Profile of MSE polarization angle along the major radius.*

worked successfully. In this system, the location of island center is evaluated by using the electron temperature perturbations (δT_e) measured with electron cyclotron emission (ECE) diagnostic as shown in Fig. 4 (b). Then the injection angle of EC wave is determined so that the EC wave deposits its power at the island center taking into account the shape of q=3/2 surface as shown in Fig. 4 (a). Waveforms of a discharge where the NTM was suppressed by using the system are shown in Fig. 4 (c). The 3/2 NTM decreased gradually and it was completely stabilized after the start of EC injection. Even after the turn-off of EC injection, the 3/2 NTM did not appear until t = 10.8 s. The β_N increased from 1.5 to 1.67, which indicated that the energy confinement was improved by the NTM suppression.

4. Current Profile Control in Reversed Shear Plasmas

4.1. Current Hole and High Performance Reversed Shear Plasma

We observed that an equilibrium with a nearly zero current density in the core or the "current hole" persisted stably for several seconds in a reversed shear plasma of I_p = 1.35 MA and q_{95} =5.2 [13] by using upgraded MSE system and equilibrium code. The q profile of higher I_p reversed shear plasma with higher fusion performance was measured and reconstructed in 2001. The profiles of MSE polarization angle, T_i, T_e, q and j are shown in Fig. 5. The MSE polarization angle shown in Fig. 5 (c), which is proportional to B_z/B_t, is very close to zero near the axis and the existence of current hole extended to a normalized radius of 0.3-0.35 was confirmed as shown in q and j profiles in Fig. 5 (b). The T_i and T_e profiles are nearly flat inside the current hole indicating poor confinement in the current hole. It is noted that, however, the flat portions in T_i and T_e profiles extended beyond the current hole radii, which cannot be explained in terms of the small poloidal field. The high temperature plasma ($T_i \sim$ 18 keV, $T_e \sim$10 keV) in the current hole was confined by off-axis poloidal field and the ITB. In this discharge, T_e ITB and the current hole were established by EC heating in a low I_p phase with a limiter configuration and they were maintained during the I_p ramp. The discharge terminated in a disruptive beta collapse when q_{min} became less than 2. Just before the collapse we achieved the DD neutron production rate = 4.6×10^{16} /s, β_N = 1.6, τ_E = 0.89 s, H_{89} = 3.0 and Q_{DT}^{eq} = 1.2 with I_p = 2.60 MA and q_{95} = 3.3 (see Table I). Hence it was
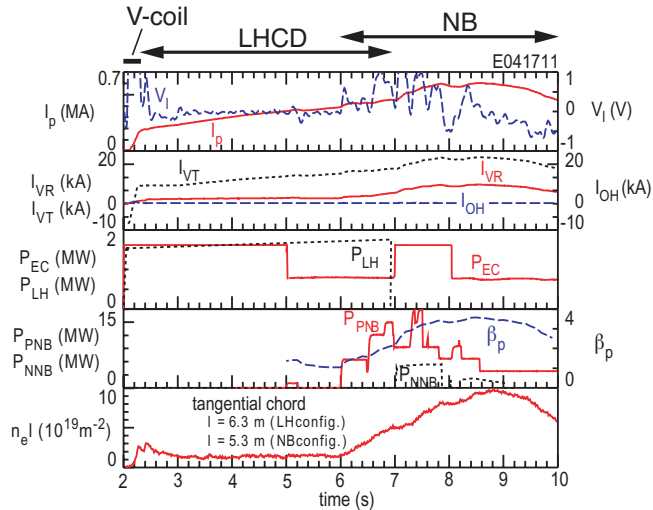
FIG. 6. A discharge where integrated scenario from the plasma startup to advanced tokamak plasma with ITBs was demonstrated. From the top, plasma current I_p and surface loop voltage V_l, OH coil current (I_{OH}) and vertical field coil current (I_{VR}, I_{VT}), LH and EC power, P-NB power, N-NB power and β_p, line-integrated electron density along a tangential chord.

confirmed that the current hole was compatible with a high I_p, low q, high performance plasma. In this discharge, the value of q_{min} at the time of major collapse has been decreased from ~1.85 to ~1.7, and the duration of high fusion performance has been extended. As a result, we were able to maintain the DT-equivalent fusion power gain of 0.8 for 0.55 s. The time derivative of the plasma stored energy was small and the ratio of DT-equivalent fusion power to the absorbed NB power reached 0.8, which is the highest value in JT-60U.

No significant negative central current density has been observed so far. Furthermore, no current is generated with ECCD or NBCD in the center of current hole [14]. These observations of clamping central current density at zero level suggest that the current hole is not a result of a transient zero inductive field near the axis, but rather of some kind of self-organized structure. The response of current profile to various kinds of current drive, EC, NB and OH, in a plasma with a current hole is under investigation to establish the method for current profile control in such a discharge.

4.2. Plasma Current Start-up without Use of OH Coil

In a steady-state tokamak reactor, the plasma current is driven mainly (>~70%) by the bootstrap current and the rest is by NBCD and/or RFCD without use of OH coils [15]. Full no-inductively driven plasmas with high bootstrap current fraction have been obtained experimentally [16,17]. However, even in these discharges, the OH coil was used to start the tokamak discharge and ramp up the plasma current. If the plasma start-up and I_p ramp-up, in addition to I_p sustainment, are accomplished without the use of OH coil, the OH coil can be removed from tokamak reactors and the substantial improvement in the economic competitiveness is expected as the machine size is reduced at a higher magnetic field [18,19]. The first demonstration of plasma start-up, I_p ramp-up, and subsequent transition to a high-performance advanced tokamak plasma without the use of the OH coil has been successfully achieved in JT-60U. Waveforms of a typical discharge are shown in Fig. 6. In this discharge, a plasma with I_p = 0.2 MA was formed at t = 2.2 s by a combination of EC preionization and induction by vertical field coils (VR and VT coils). Subsequently, I_p was ramped up by LHCD until t = 6 s when I_p reached 0.4 MA. Finally, NB injection was started to raise the plasma beta. The plasma stored energy was feedback controlled by using the P-NB power, which resulted in an irregular shape in P-NB power waveform in Fig. 6. The increased β_p is expected to be effective to raise I_p through the flux provided by the increased current in vertical field coils. The highest plasma current achieved so far in this scenario is 0.7 MA. The ITB and the edge transport barrier (H-mode) were obtained with NB heating. The radius of ITB was large and high confinement, HH_{y2}=1.6, was obtained with β_p = 3.6 and β_N=1.6. The q profile was reversed with the normalized radius of q_{min} of 0.7 and the current hole existed in
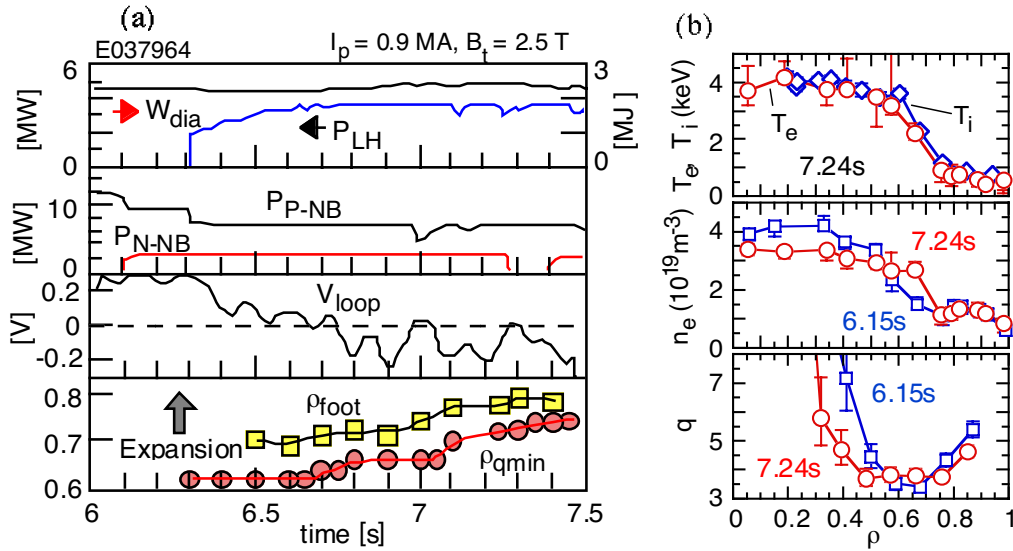
FIG.7. (a) Waveforms and (b) profiles of a reversed shear discharge in which the current profile was controlled with LHCD and NBCD in full non-inductive current drive. In (a), from the top, LH power, plasma stored energy, P-NB power, N-NB power, surface loop voltage, normalized raidus of ITB foot (ρ_{foot}) and that of q_{min} (ρ_{qmin}). In (b), from the top, T_i and T_e profiles at t = 7.24 s, n_e profiles at t=6.15 and 7.24 s, q profiles at t=6.15 and 7.24 s.

the center. An interesting point is that the current hole seems to be already formed before NB heating, namely during the LHCD phase. This may imply that the current hole will also be formed in future reactors if this scenario is employed and that the control of current profile in a plasma with the current hole is important.

4.3. Current Profile Control in Reversed Shear Plasmas

The active modification of current profile in a reversed shear plasma with a large bootstrap current fraction was demonstrated by using LHCD and NBCD [20]. Waveforms of a typical discharge are shown in Fig. 7 (a). The reversed shear q profile and the ITB were established with P-NB heating during I_p ramp-up. Injection of N-NB and LH started at t = 6.1 s and 6.3 s, respectively. The surface loop voltage started to decrease after the injection of LH and reached -0.2 V. The internal loop voltage evaluated with the MSE measurement was also negative in the whole plasma volume. This indicates that the plasma current was entirely driven by the non-inductive current. The bootstrap current was estimated 62% of the plasma current and the rest was provided by LHCD and NBCD. High confinement (HH_{y2} = 1.4) and high beta (β_N=2.2) was maintained at a high normalized density (n_e-bar/n_{GW} = 0.8) under the full non-inductive current drive. The high confinement and high beta are supposed to be due to the large ITB radius as shown in Fig. 7 (b) [21]. The normalized radius of q_{min}, ρ_{qmin} increased from t = 6.6 s as shown in the bottom panel of Fig. 7 (a). This is due to the off-axis current drive by LH and is in clear contrast to the case without LHCD where ρ_{qmin} continued to shrink due to the penetration of inductive current. The radius of T_i ITB foot, ρ_{foot}, increased as the ρ_{qmin} was expanded. From the q profiles shown in Fig. 7 (b), it is also noted that the q values inside the ITB, ρ<0.5, was decreased. This is not due to the penetration of inductive current but due to the central current drive with N-NB because the loop voltage in this region was negative. The reduction in q in the central region is effective to improve the confinement of high energy particles including α particles in fusion reactors. Therefore, we have demonstrated that the q profile can be modified favorably by means of combined external non-inductive current drive even with a high bootstrap current fraction.

5. Internal Transport Barrier

Major issues for the application of the internal transport barrier to ITER or demo reactors are (i) ITB formation condition and ITB control, (ii) formation of electron ITB to improve the electron confinement, (iii) sustainment of ITBs, especially the ion ITB, under the reactor-relevant conditions, with dominant electron heating and small central particle fueling, and (iv) impurity accumulation in ITB. Recent JT-60U research on ITB has focused on these items.

Formation of ITB in weak positive shear and reversed shear plasmas was studied by varying the heating power systematically. The relation between the thermal diffusivity (χ_i and χ_e) and the radial electric field shear (E_r shear) was investigated extensively [22]. It is found that in the weak ITB χ_i decreases gradually with the increase of heat flux density and the E_r shear. In positive shear plasmas, there was a threshold heating power for formation of weak ITB while no threshold power was found in reversed shear plasmas. In both of positive shear and reversed shear plasmas, the strong (box-type) ITB was formed with a bifurcation or a sudden drop in χ_i as a function of time or E_r shear. The critical value of E_r shear for the transition to the strong ITB was found to increase with the poloidal magnetic field.

The electron ITB is important to improve the energy confinement in ITER and demo reactors in which the electron heating power is dominant and T_i is expected to be lower than T_e. The electron ITB also attracts attention recently since it is considered that the formation mechanism of electron ITB is different from that of ion ITB [23]. The improved performance of EC heating in JT-60U enables us to investigate the formation of electron ITB in a wide range of electron heating power. The electron ITB formation in low T_i, low beta plasmas was investigated by injecting the EC wave into a low density plasma with zero or small NB heating power. In reversed shear plasmas, the normalized inverse scale length of T_e, R/L_{Te} increased with EC heating power and exceeded 20 with 3 MW heating. On the other hand, in weak positive shear plasmas, R/L_{Te} stayed constant (~10) up to 3 MW. These results indicate that the electron ITB is formed with a small heating power in reversed shear plasmas but is not formed in positive shear plasmas with the present available electron heating power. An electron ITB with high T_e (~ 25 keV) in a wide region (~30% of plasma minor radius) was obtained with EC heating in a reversed shear plasma sustained by the LH current drive [24]. It is noted that the electron ITB in reversed shear plasmas was already observed in previous JT-60U experiments where LHRF was employed for electron heating and formation of reversed shear [25]. When high power NB heating was applied to EC heated plasmas, the situation was
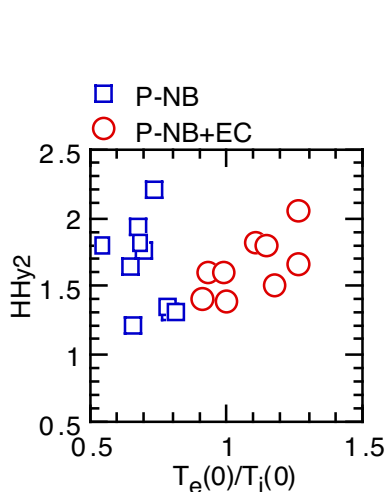
FIG. 8. HH factor as a function of T_e/T_i in reversed shear plasmas. Squares denote P-NB heated discharges while circles denote P-NB + EC heated discharges.
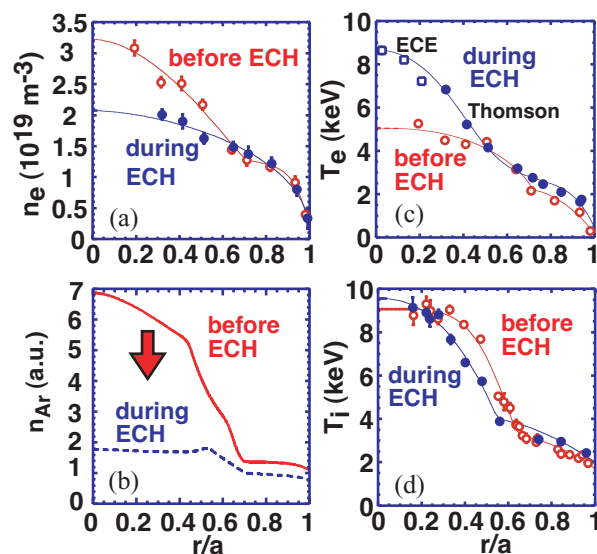
FIG. 9. Ar exhaust with EC heating in a high β_p mode plasma. Profiles of (a) n_e, (b) Ar density, (c) T_e and (d) T_i before and during EC heating.

different. Both in weak positive shear and reversed shear plasmas, the electron ITB was formed at the similar location to ion ITB. This implies that the large pressure gradient or E_r shear accompanied by the ion ITB affects the formation of electron ITB.

As for item (iii), sustainment of ITB in the reactor-relevant regime, effects of electron heating on the ion ITB were mainly investigated [20]. The increased T_e/T_i may cause an increase of growth rate of ion temperature gradient (ITG) mode and enhancement of ion transport. In a reversed shear plasma with box-type ITBs, heat and particle barriers for ions and electrons were sustained in a regime with $T_e >\sim T_i$. The HH factor, HH_{y2}, is plotted as a function of T_e/T_i in the central region in Fig. 8. High confinement with $HH_{y2}>\sim 1.5$ was obtained even in a regime with $T_e>T_i$ in reversed shear plasmas. In E41738, $HH_{y2} = 2.05$, which is among the highest values in JT-60U plasmas, was obtained with $T_e/T_i = 1.3$. In this discharge, EC heating power was 2.6 MW, which corresponded to 44% of total heating power. The ITB foot and q_{min} were located around $\rho\sim 0.6$ and the box-type ITB with a very narrow ITB layer (5-10 cm) was observed. The efficient heating inside the ITB shoulder with EC may be related to the high confinement. The parameters in E41738 are listed in Table I. On the other hand, the decrease in T_i gradient and the toroidal rotation shear were often observed when the EC wave was injected into a weak positive shear plasma with parabolic type ITBs. In positive shear plasmas, ion ITB with $T_e>T_i$ was not obtained. It is noted, however, the NB heating power was limited below ~15 MW in this experiment so as to achieve $T_e>T_i$ with available EC power. Sustainment of ITB in a regime of $T_e>T_i$ will be attempted using higher electron heating power, for instance injecting N-NB in addition to EC, in future.

Impurity accumulation is one of the largest issues for application of ITB to reactors. Transport of various impurities (He, C, Ar) and bulk particles have been investigated in weak and strong ITB plasmas [26]. It was found that diffusivities of impurities and electrons were strongly correlated with the heat transport or χ_i in a wide range of χ_i, $1< \chi_i/\chi_i^{NC}<10$. In a plasma with a strong ITB with $\chi_i\sim\chi_i^{NC}$, heavier impurities tended to accumulate but the peaking factor in the profile shape was smaller than the values from neoclassical prediction for C and Ar. When EC was injected into a high β_p mode plasma after Ar puff, the electron density was reduced and Ar was exhausted. The profiles before and during EC injection are shown in Fig. 9. The density ITB was almost lost during EC heating while the ion ITB was maintained. The profile of Ar was evaluated from the profile of soft X-ray emission. The exhaust of Ar can be explained by the reduction of inward velocity of Ar caused by reduction of n_e gradient in neoclassical transport. This indicates that it is important to control the density gradient for the control of impurity accumulation.

ITB control through perturbation in density or temperature or magnetic field was also attempted [27]. Reduction of density fluctuation and improvement of confinement was observed when a pellet was injected into reversed shear plasmas [26]. The role of rational q values in the non-local transport bifurcations inside and around the ITB, ITB event, has been investigated [28].

6. ECCD Study

The ECRF current drive is considered a powerful tool for the local current profile control and suppression of NTM. In JT-60U, localized current drive, consistent with the linearized Fokker-Planck calculation [29], was confirmed with the MSE measurement [30]. In ITER or demo reactors, ECCD in high n_e and high T_e plasmas is required. Furthermore, the location of ECCD should be varied from the axis to the off-axis ($\rho<\sim 0.6$) region. To evaluate the current drive efficiency η_{CD} in a high T_e regime, a high T_e plasma was produced with high power EC heating up to 3 MW in a low density regime ($n_e\sim 0.5\times 10^{19}m^{-3}$). To evaluate η_{CD} experimentally, it is required to avoid MHD instability and sustain high T_e stably. By optimizing the target current profile and EC deposition location, a stable high T_e plasma was obtained where $T_e(0) \sim 23$ keV was maintained for 0.8 s. The evaluated η_{CD} increases with T_e but the value was lower than the linearized Fokker-Plank calculation in the high T_e regime ($T_e \sim 20$ keV). This is considered due to the negative toroidal electric field induced by the large
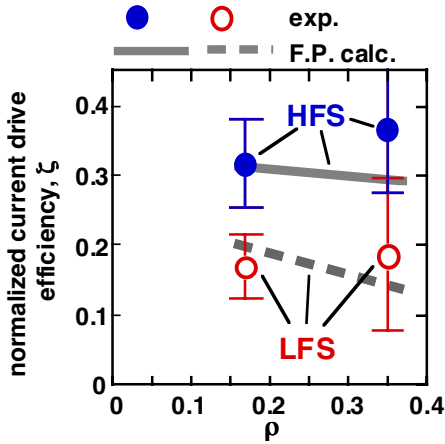
FIG. 10. Normalized EC current drive efficiency ζ as a function of normalized radius for deposition locations at the high-field-side (HFS) and the low-field-side (LFS). Open and closed circles denote measured values and solid and dotted lines denote the results of linearized Fokker-Plank calculation.
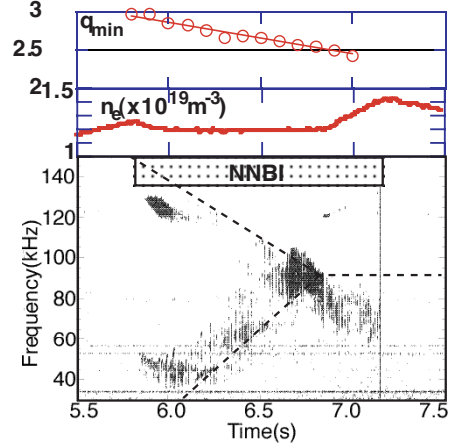

FIG. 11. Alfvén eigenmode observed in a reversed shear plasma with N-NB injection. From the top, q_{min}, line-averaged electron density, frequency spectrum of magnetic fluctuation. The dotted lines in the bottom indicate the predicted frequency of reversed-shear-induced Alfvén eigenmode.

EC driven current density, j_{EC} [31]. To evaluate η_{CD} precisely, a higher density plasma with high T_e is required to reduce j_{EC}. In off-axis CD, the effect of trapped electrons was found by changing the EC deposition position in the poloidal direction as shown in Fig. 10. The dependence on n_e and T_e was also investigated and a strong dependence on n_e was found in the range of $(1-1.8) \times 10^{19}$ m^{-3}. This is considered due to the enhanced coupling to increased number of fast electrons.

7. Alfvén Eigenmode

In the Alfvén eigenmode (AE) study, a new model has been found consistent with the observed frequency sweep and saturation during N-NB injection in reversed shear plasmas [32]. In the discharge shown in Fig. 11, the hydrogen N-NB of 360 keV and 4 MW was injected into a reversed shear plasma with $B_t = 3.7$ T and $I_p = 1.3$ MA. Magnetic fluctuations in the AE frequency range have been observed during N-NB injection. Only the n=1 mode was observed due to relatively small fast ion beta (<0.2%). The frequency chirp both in upward and downward directions was observed. The dotted lines are frequencies of the shear AE near the zero shear region of reversed shear plasma, which is called the reversed-shear-induced AE (RSAE). The frequency of RSAE depends strongly on the value of q_{min} and it can explain the observed frequency chirp very well as shown in Fig. 11. The AE frequency saturates at t = 6.65-6.85 s and the amplitude was enhanced. This can be explained by the transition of RSAE to TAE which occurs at q_{min} ~2.5. To avoid these large amplitude TAEs, it is suggested to operate a reversed shear plasma outside the range of this transition, for instance $2.4 < q_{min} < 2.7$. The RSAE can also explain the previously observed rapid frequency sweeping modes with n>1 in JT-60U ICRF heated reversed shear plasmas [33].

8. H-mode and ELM Study

In the H-mode pedestal regime, important points are to maintain high confinement in the high density regime and to reduce the ELM heat load to the target plates.

In Ar-seeded H-mode plasmas, higher confinement is obtained in the high density regime than no impurity-seeded plasmas. A higher pedestal ion temperature is obtained with a fixed pedestal pressure in Ar-seeded plasmas where the ion density is lower, and this results in a

higher core temperature and higher confinement though the profile stiffness [34]. The reduction of instability growth rates with an increase of Z_{eff} may also be involved [35]. In JT-60U, a configuration with the outer strike point located on the dome-top ("dome-top configuration") was found to enhance the confinement further [36]. With this configuration, giant ELMs disappeared in the high density regime and the heat load due to ELMs decreased to 1/10 compared to the low density case. In 2002, high power N-NB injection extended the density regime to n_e-bar/n_{GW} = 0.95 keeping HH_{y2}~0.9 as shown in Fig.12. The parameters of this discharge (E41536) are listed in Table I.

It is very important to raise the pedestal pressure in order to enhance the global stability and confinement properties. We have found that the pedestal pressure increased by a factor of 2-2.5 with total (or core) poloidal beta in high triangularity (δ~0.45) plasmas with type I and type II ELMs as shown in Fig. 13 [37]. As a result, high confinement of HH_{y2} = 1.1 was achieved at n/n_{GW} = 0.7 in a pellet injected discharge. An increase in the pedestal pressure was not caused by an increase of the pedestal width but by an increase of the pressure gradient (α parameter) at the pedestal. In contrast, the pressure and the α parameter at the pedestal stayed almost constant in low δ plasmas. The pedestal pressure in high δ H-mode plasma increases gradually in time even with constant β_p. This is considered to be due to the change of local magnetic shear by the edge bootstrap current.

The type II ELM, with a small heat load onto the divertor plates, appears in a high δ and high q_{95} region. By increasing δ up to 0.6, the type II ELMy regime has been expanded to a lower q regime (q_{95} =3.8). In this region, the type II ELM was maintained during pellet injection while type I ELM appears after each pellet with a smaller δ(~0.45) or q_{95}.

The dynamics of density collapse due to type I ELMs was measured using a reflectometer [38]. The time scale (100-350 μs), penetration depth (11 cm or twice the pedestal width) and a poloidally asymmetric structure of the collapse were observed. It was revealed that the ELM heat load is mainly carried by the convective transport using SOL Mach probes and IRTV.

Understanding of SOL flow pattern and the driving mechanism is crucial for particle and impurity control in divertor. A new reciprocating Mach probe has been installed above the high-field-side baffle plate and SOL measurement at three locations (high-field-side, low-field-side and X-point) has been made possible. The SOL flow measurements revealed the importance of ExB drift flow [39]. As for the plasma-surface interaction, tritium retention of the first wall materials has been studied by analyzing the carbon tiles [40,41].
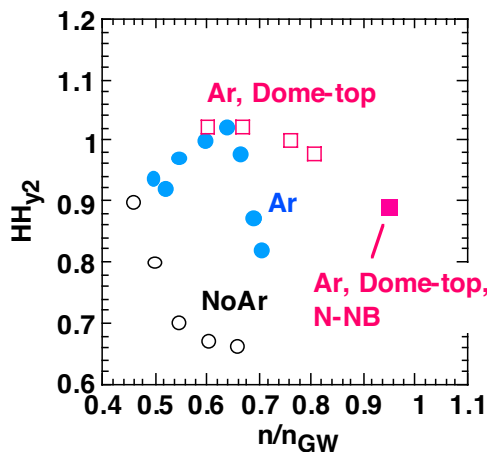

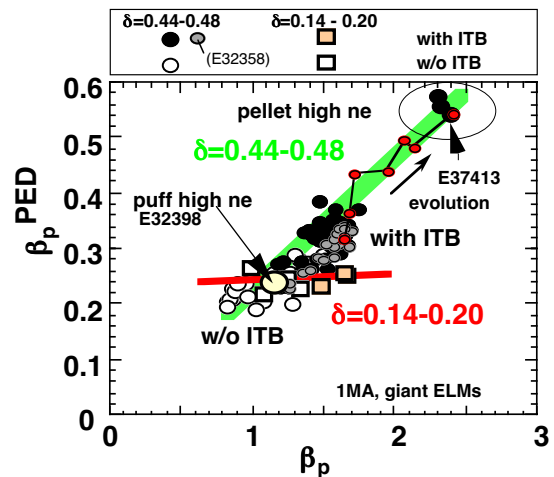FIG. 12. HH factor as a function of normalized density in ELMy H-mode.

FIG. 13. Pedestal β_p as a function of total β_p in H-mode plasmas with high and low δ.

TABLE I. Parameters of typical discharges

Shot	39713	40259	37964	41738	41536
mode	High β_p H, Full CD	RS, Q_{DT}^{eq} =0.8x0.55s	RS, Full CD	RS, High HH with $T_e>T_i$	Ar-seeded H, Dome-top, High n_e
time [s]	6.5	7.22	7.24	6.5	9.0
I_p [MA]	1.795	2.6	0.90	1.3	1.20
B_t [T]	4.09	4.32	2.52	3.71	2.50
P_{aux}^{abs} [MW]	21.8	13.035	9.00	5.87	17.0
R_p [m]	3.226	3.101	3.51	3.34	3.33
a [m]	0.776	0.717	0.952	0.78	0.88
q_{95}	4.1	3.26	6.9	5.08	4.23
κ_x	1.548	1.86	1.38	1.55	1.46
δ_x	0.34	0.05	0.45	0.26	0.35
W_{dia} [MJ]	7.495	8.427	2.45	3.58	2.82
dW_{dia}/dt [MW]	~0	4.38	0.36	1.34	0.47
S_n [10^{16}/s]	3.6	4.57	0.23	0.22	0.60
Z_{eff}	3.0	3.25	3.44	3.0	3.22
$n_e(0)$ [$10^{19}m^{-3}$]	6.77	9.9	3.4	4.3	8.0
$n_D(0)$ [$10^{19}m^{-3}$]	4.2	5.44	1.7	2.4	6.2
n_e-bar [$10^{19}m^{-3}$]	~4.0	5.49	2.59	3.16	4.70
n_e-bar/n_{GW}	0.42	0.34	0.82	0.47	0.95
$T_i(0)$ [keV]	21.5	18.07	4.0	7.36	~6
$T_e(0)$ [keV]	10.5	10.04	4.0	9.32	~4
τ_E [s]	0.344	0.887	0.28	0.75	0.17
H_{89PL}	2.53	2.95	2.45	3.47	1.58
HH_{y2}	1.22	1.55	1.39	2.05	0.89
β_N	2.40	1.61	2.17	1.72	2.06
β_p	1.73	1.01	2.10	1.57	1.43
β_t [%]	1.37	1.35	0.81	0.77	1.12
f_{BS}	0.50	-	0.62	0.56	0.37
$f_{NBCD/RFCD}$	0.50	-	>0.38	0.12	-
P_{rad}/P_{net}	0.54	-	-	0.43	0.8

9. Summary and Discussions

Enhanced capabilities of N-NB and ECH enabled the research approaching the reactor-relevant regime including high $n\tau T$ full non-inductive CD, NTM stabilization, current profile control in reversed shear plasmas, high confinement reversed shear plasma with $T_e>T_i$ and high confinement at the high density. Achieved parameters of typical discharges are listed in Table I. A new operation scenario has been established in which a plasma with high bootstrap current fraction and ITBs is produced without using OH coil. Significant advance in physics understanding on a high temperature plasma has been obtained including discovery of the current hole, measurement of ELM dynamics and a new type of AE mode.

Studies on the ITB and the edge pedestal were intensively carried out with emphasis on reactor-relevant conditions. Impurity accumulation related to large density gradient in strong ITBs in a reversed shear plasma and degradation of ITB by ECH in a weak positive shear plasma have been found. In order to decide what type of ITB and q profile are suitable in reactors, experiments with low particle fueling condition, in addition to the dominant electron heating, will be important.

In future, we will continue to develop discharges with higher integrated performance with improvement of N-NB, pellet and EC. Extensive physics study will also be performed in enhanced collaboration with other institutes.

References

[1] ISIHIDA, S., et al., in Fusion Energy 1996 (Proc. 16th Int. Conf. Montreal, 1996), Vol. 1, IAEA, Vienna (1997) 315
[2] KAMADA, Y., et al., Nucl. Fusion **39** (1999) 1845.
[3] FUJITA, T., et al., Nucl. Fusion **38** (1998) 207.
[4] KAMADA, Y., et al., Fusion Science Tech. **42** (2002) 185.
[5] KOIDE, Y., et al., Phys. Rev. Lett. **72** (1994) 3662.
[6] FUJITA, T., et al., Phys. Rev. Lett. **78** (1997) 2377.
[7] KAMADA, Y., JT-60 Team, Nucl. Fusion **41** (2001) 1311.
[8] UMEDA, N., this conference, CT-6Rd.
[9] KIZU, K., et al., Fusion Eng. Des. **58-59** (2001) 331.
[10] TAKENAGA, H., Phys. Plasmas **8** (2001) 2217.
[11] ISAYAMA, A., this conference, EX/C2-2.
[12] ITER, Final Design Report, Plant Description Document.
[13] FUJITA, T., et al., Phys. Rev. Lett. **87** (2001) 245001.
[14] MIURA, Y., et al., this conference, EX/C3-1Ra.
[15] KIKUCHI, M., Nucl. Fusion **30** (1990) 265.
[16] FUJITA, T., et al., Phys. Rev. Lett. **87** (2001) 085001.
[17] HOBIRK, J., et al., Phys. Rev. Lett. **87** (2001) 085002.
[18] NISHIO, S., et al., in Fusion Energy 2000 (Proc. 18th Int. Conf. Sorrento, 2000) IAEA-CN-77/FTP2/4/
[19] NISHO, S., et al., this conference, FT/P1-21.
[20] IDE, S., et al., this conference, EX/C3-3.
[21] TAKIZUKA, T., et al., Plasma Phys. Controlled Fusion **44** (2002) A423.
[22] SAKAMOTO, Y., et al., this conference, EX/P2-08.
[23] DOYLE, E.J., et al., Nucl. Fusion **42** (2002) 333.
[24] IKEDA, Y., et al, "Formation of high electron temperature plasmas in ECH experiments on JT-60U tokamak," in 12th Joint Workshop on Electron Cyclotron Emission and Electron Cyclotron Resonance Heating, Aix-en-Provence, 2002.
[25] IDE, S., et al., in Fusion Energy 1996 (Proc. 16th Int. Conf. Montreal, 1996), Vol. 3, IAEA, Vienna (1997) 253.
[26] TAKENAGA, H., et al., this conference, EX/C3-5Rb.
[27] FUKUDA, T., et al., to be published in Plasma Phys. Control. Fusion.
[28] NEUDATCHIN, S.V., et al., this conference, EX/P2-06.
[29] HAMAMATSU, K., et al., Fusion Eng. Design **53** (2000) 53.
[30] SUZUKI, T., et al., Plasma Phys. Controlled Fusion **44** (2002) 1.
[31] SUZUKI, T., et al., this conference, EX/W-2.
[32] TAKECHI, M., et al., this conference, EX/W-6.
[33] KIMURA, H., et al., in Fusion Energy 1996 (Proc. 16th Int. Conf. Montreal, 1996), Vol. 3, IAEA, Vienna (1997) 295.
[34] KUBO, H., et al., Nucl. Fusion **41** (2001) 227.
[35] HILL, K.W., et al., this conference, EX/P2-03.
[36] HIGASHIJIMA, S., et al., in Proc. of 15th International Conference on Plasma Surface Interactions in Controlled Fusion Devices, I-03, to be published in J. Nucl. Mater.
[37] KAMADA, Y., et al., this conference, EX/P2-04.
[38] OYAMA, N., et al., this conference, EX/S1-1.
[39] ASAKURA, N., et al., this conference, EX/D1-3.
[40] TANABE, T., et al., in Proc. of 15th International Conference on Plasma Surface Interactions in Controlled Fusion Devices, I-06, to be published in J. Nucl. Mater.
[41] TANABE, T., et al., this conference, EX/P2-11.